Available online at www.sciencedirect.com
ScienceDirect
Journal of Solid State Chemistry 181 (2008) 298–305
JOURNAL OF SOLID STATE CHEMISTRY
www.elsevier.com/locate/jssc

Phase segregation in mixed Nb–Sb double perovskites $Ba_2LnNb_{1-x}Sb_xO_6$

Paul J. Saines, Brendan J. Kennedy*

School of Chemistry, The University of Sydney, Sydney, NSW 2006, Australia

Received 6 September 2007; received in revised form 19 November 2007; accepted 27 November 2007
Available online 5 December 2007

Abstract

The phase composition of two series of mixed Nb^{5+}–Sb^{5+} double perovskites formed between the pairs Ba_2EuNbO_6–Ba_2PrSbO_6 and Ba_2NdSbO_6–Ba_2NdNbO_6 have been studied using synchrotron X-ray powder diffraction methods. In both series extensive phase segregation is observed demonstrating limited solubility of Sb^{5+} in these Nb^{5+} perovskites, irrespective of the precise structures of the double perovskite. Evidence for a monoclinic $I2/m$ phase in the series formed between tetragonal $I4/m$ Ba_2EuNbO_6 and rhombohedral $R\bar{3}$ Ba_2EuNbO_6 is presented. It is postulated that this phase segregation is a consequence of competing bonding requirements of the Nb^{5+} and Sb^{5+} cations associated with their electronic configurations.

Keywords: Perovskite; Phase segregation; Rietveld refinement

1. Introduction

Metal oxides with the double perovskite structure continue to attract attention due to the diverse range of properties exhibited by these materials including colossal magneto-resistance, ionic conductivity, ferro- and piezo-electricity and ferromagnetism [1]. Such properties are known to be strongly influenced by the precise structure of the oxides, as exemplified by the recent illustration of switching from ferromagentism to antiferromagnetism in A_2CrSbO_6 by Retuerto et al. [2]. Consequently structural studies of such perovskites are pivotal in understanding these important physical properties. In particular, properties such as colossal magneto-resistance and ferroelectricity tend to be most prominent in compounds close to a structural instability that may take the form of a phase transition or a solubility limit [3]. This is extremely well documented for ferroelectrics based on Pb–Zr–Ti perovskites (PZT) where optimal performance occurs near the morphotropic phase boundary [4,5]. The diverse range of structures adopted by perovskites and the presence of structural, electronic and magnetic phase transitions between these demonstrates a greater complexity in the structure and chemistry of these oxides than may be naively expected from the relatively simple structure of the parent primitive cubic perovskite.

The chemistry and structures of perovskites containing Nb^{5+} and Sb^{5+} provide a number of examples of unexpected structural complexity [6–9]. The similar charge and ionic radii of Sb^{5+} (0.60 Å) and Nb^{5+} (0.64 Å) [10] lead to the assumption that antimonate and niobate compounds should adopt similar perovskite structures. There are, however, numerous examples in the perovskite family where the niobate and antimonate compounds adopt different structures or where the antimonate but not the corresponding niobate, or vice versa, forms. Examples where the antimonate but not the corresponding niobate exists include Ba_2BiSbO_6 [11] and $Ba_4NaSb_3O_{12}$ [12] while the Aurivillius phase $BaBi_2Nb_2O_9$ [13] is known to exist but $BaBi_2Sb_2O_9$ is unknown. The series $Ba_2LnB'O_6$ (Ln = lanthanide and $B' = Nb^{5+}$ or Sb^{5+}) provides an unusual example of perovskite-type oxides where both the antimonate and niobate form, but these adopt different structures. Both series undergo a sequence of phase transitions with decreasing average ionic radii of the

*Corresponding author. Fax: +61 2 9351 3329.
E-mail address: kennedyb@chem.usyd.edu.au (B.J. Kennedy).

0022-4596/$ - see front matter © 2007 Elsevier Inc. All rights reserved.
doi:10.1016/j.jssc.2007.11.035

B-site cations from $I2/m$ monoclinic (Glazer tilt system $a^-a^-c^0$ [14,15]) to an intermediate structure and then ultimately to $Fm\bar{3}m$ cubic ($a^0a^0a^0$) symmetry [7]. The intermediate structure adopted by the two series is, however, different with the antimonates having a $R\bar{3}$ rhombohedral ($a^-a^-a^-$) intermediate while the majority of niobates adopt an $I4/m$ tetragonal ($a^0a^0c^-$) structure [6,7]. The differences in the physio-chemistry and structure of antimonate and niobate perovskites indicates that factors other than ionic radii and valency play an important role in the formation and stability of the resulting perovskites.

Understanding of the chemical basis for the differences between Nb^{5+} and Sb^{5+} containing perovskites is clearly needed. Although superficially similar and having near identical tolerance factors the two oxides Ba_2PrSbO_6 and Ba_2EuNbO_6 (tolerance factors of 0.795 and 0.794, respectively [1]) adopt alternate intermediate structures, $R\bar{3}$ and $I4/m$, respectively, at room temperature. Structural studies of solid solutions of the type $Ba_2Eu_{1-x}Pr_xNb_{1-x}Sb_xO_6$ are, therefore, expected to shed light on the chemical differences between Nb^{5+} and Sb^{5+} while also providing further insight into the complex phase transition behaviour in $Ba_2LnB'O_6$ oxides. A related study by Mitchell and co-workers [16] on the series $Sr_{1-2x}Na_xLa_xTiO_3$ (solid solution between $SrTiO_3$ and $Na_{0.5}La_{0.5}TiO_3$) concluded that the transition from $I4/mcm$ to $R\bar{3}c$ occurs directly via a discontinuous phase transition [17]. The $I4/mcm$ to $R\bar{3}c$ transition in these ABO_3 perovskites involves the same two Glazer tilt systems, $a^0a^0c^-$ and $a^-a^-a^-$, as an $I4/m$ to $R\bar{3}$ transition that may occur in the $A_2BB'O_6$ double perovskite series $Ba_2Eu_{1-x}Pr_xNb_{1-x}Sb_xO_6$. The difference in symmetry between the two series is a consequence of the ordering of the two different *B*-site cations in $Ba_2Eu_{1-x}Pr_xNb_{1-x}Sb_xO_6$. Interestingly the $I4/mcm$ phase is not observed in the series $La_{1-x}Sr_xCr_{1-x}Ti_xO_3$ where a first-order transition from $Pnma$ to $R\bar{3}c$ occurs [18].

The tetragonal to rhombohedral phase transition in $Ba_2Eu_{1-x}Pr_xNb_{1-x}Sb_xO_6$ may be first order, as seen for $Sr_{1-x}Na_xLa_xTiO_3$, or it may involve an intermediate phase. This would most likely be either $I2/m$ monoclinic ($a^-a^-c^0$) or $Fm\bar{3}m$ cubic ($a^0a^0a^0$), both of which are observed in the two $Ba_2LnB'O_6$, $B' = Nb^{5+}$ or Sb^{5+}, series. Alternatively, the different structures observed for Ba_2PrSbO_6 and Ba_2EuNbO_6 may indicate that Nb^{5+} and Sb^{5+} are incompatible in the same perovskite structure. Such incompatibility could manifest itself as a solubility gap that would lead to segregation and the formation of two or more phases with different chemical compositions. Such segregation would be consistent with the apparent chemical incompatibility of niobium and antimony perovskites mentioned previously.

In order to determine which of these three possibilities (direct first-order phase transition, presence of an intermediate phase or phase segregation) occurs we have synthesized two series of oxides, namely $Ba_2Eu_{1-x}Pr_xNb_{1-x}Sb_xO_6$ and $Ba_2NdNb_{1-x}Sb_xO_6$ and structurally characterized these using synchrotron X-ray diffraction and, as required, analytical electron microscopy. These oxides were chosen to minimize the changes in volume and tolerance factor across the series. That is, the only significant difference across each series will be the exchange of Sb^{5+} for Nb^{5+}. The resolution and high intensity offered by synchrotron X-ray powder diffraction makes it easier to resolve the splitting of peaks in perovskites, particularly those that appear to be pseudo-cubic, allowing the symmetry of compounds to be determined. High resolution is also important in determining whether the samples consist of single or multiple perovskite phases.

2. Experimental

All starting materials were obtained from Sigma-Aldrich Chemicals. The lanthanide oxides and barium carbonate were dried prior to use by heating at 1000 and 100 °C overnight. Samples of $Ba_2Eu_{1-x}Pr_xNb_{1-x}Sb_xO_6$ and $Ba_2NdNb_{1-x}Sb_xO_6$ ($x = 0, 0.1, 0.2, \ldots, 1$) were prepared from stoichiometric mixtures of $BaCO_3$, Nb_2O_5, Sb_2O_3 and the appropriate lanthanide oxides; Pr_6O_{11}, Nd_2O_3 and Eu_2O_3. The appropriate starting mixtures were finely ground as an acetone slurry and, after drying, were heated for a period of 24 h at 800 °C followed by heating at 1000, 1100 and 1200 °C for periods of 24 h. The samples were then pressed into pellets and heated at 1300 °C for 24 h followed by heating, in pelleted form, for a maximum of 48 h at 1350 °C and 24 h at 1400 °C in order to yield samples with the maximum purity. In all cases samples were reground and, if required, repelleted after each heating period.

The reactions were monitored by powder X-ray diffraction using Cu-$K\alpha$ radiation on a Shimadzu X-6000 Diffractometer. Synchrotron X-ray diffraction data were recorded on the Debye Scherrer diffractometer at the Australian National Beamline Facility, Beamline 20B at the Photon Factory, Tsukuba, Japan [19]. The samples were housed in 0.3 mm capillaries that were continuously rotated during measurement to reduce the effects of preferred orientation. Data were collected using three image plates as detectors covering the range of $5 < 2\theta < 125°$ with a step size of 0.01° and a wavelength of 0.80073 or 0.80286 Å. Variable temperature measurements, at temperatures of up to 500 °C, were carried out using a custom built furnace over a range of $5 < 2\theta < 85°$.

Refinements of the crystal structures were performed with the program RIETICA [20]. The diffraction peaks were described by a pseudo-Voight function using a Howard asymmetry correction where necessary [20]. The background was estimated from interpolation between up to 40 selected points.

Scanning electron microscopy (SEM) and energy dispersive X-ray analysis (EDX) were conducted for selected samples using a Phillips XL 30 SEM with a tungsten filament operating at 25 keV and a spot size of 5 μm. The EDX operation and data analysis was performed using the DX-4eDX ZAF operating system.

3. Results and discussion

3.1. Structure of $Ba_2Eu_{1-x}Pr_xNb_{1-x}Sb_xO_6$

As expected from previous studies by our group [7] the synchrotron X-ray diffraction patterns of the end member compounds in the series $Ba_2Eu_{1-x}Pr_xNb_{1-x}Sb_xO_6$ had peak splitting and superlattice reflection conditions consistent with a $R\bar{3}$ rhombohedral structure for Ba_2PrSbO_6, $x=1$, and $I4/m$ tetragonal symmetry for Ba_2EuNbO_6, $x=0$ (see Figs. 1 and 2). This can clearly be seen in the peaks corresponding to the (400) and (444) reflections of the cubic double perovskite structure. For Ba_2PrSbO_6 the (444) reflection near $2\theta=38^\circ$ appears as a doublet but the (400) reflection near $2\theta=21.5^\circ$ remains as a single reflection, whereas for Ba_2EuNbO_6 the (444) is a single reflection and the (400) is a doublet. Subsequent refinements of models in the appropriate symmetry gave good fits to the patterns (see Table 1 for crystallographic details). The compounds with $0.5\leqslant x\leqslant 0.9$ were also found to be rhombohedral.

The diffraction patterns of the compounds with $0.1\leqslant x\leqslant 0.4$ were not well fitted by either single or two-phase models in $R\bar{3}$ and/or $I4/m$. The diffraction patterns of these compounds contained only *R*-point superlattice reflections with no evidence for any *M*- or *X*-point reflections being found. *R*-point reflections indicate the presence of out-of-phase tilting and/or cation ordering while *M*-point reflections indicate the presence of in-phase tilts and *X*-point reflections arise from a coupling of the *R*- and *M*-point modes. Discarding the tetragonal and rhombohedral structures shown not to fit the observed diffraction data, the group theoretical analysis by Howard et al. [17] indicates there are only three other possibilities that have either no tilts or only out-of-phase tilts. These are $P\bar{1}$ triclinic (tilt system $a^-b^-c^-$), $I2/m$ monoclinic ($a^-a^-c^0$) and $Fm\bar{3}m$ cubic ($a^0a^0a^0$). The diffraction patterns of the compounds with $0.1\leqslant x\leqslant 0.4$ were all inconsistent with single-phase models for any of these structures.

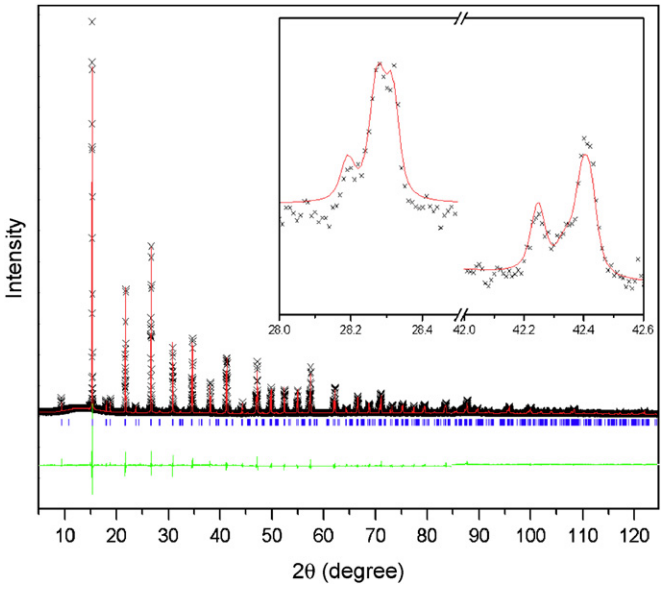

Fig. 1. Synchrotron X-ray diffraction pattern of Ba_2EuNbO_6. The insert shows some of the higher order *R*-point superlattice reflections indicating both the high intensity of these peaks, caused by the combination of cation ordering and octahedral tilting, and the low background of the data used in this study. The crosses, upper and lower continuous lines represent the observed and calculated intensities and the difference between these, respectively. The vertical markers show the positions of the allowed Bragg reflections.

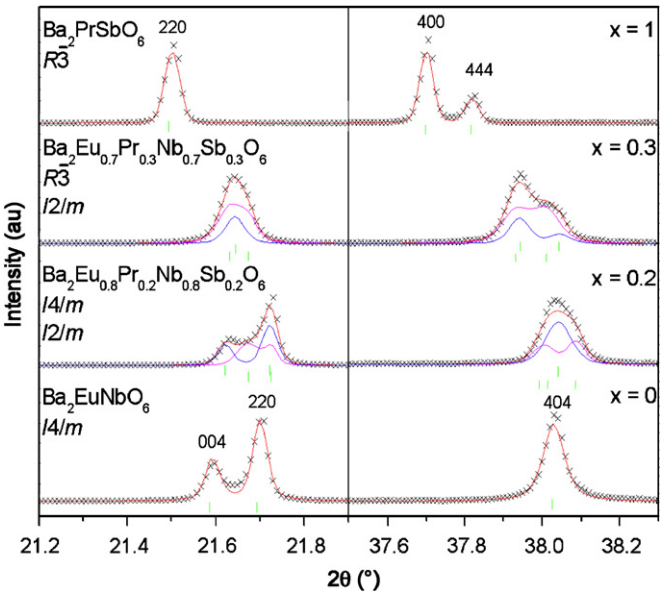

Fig. 2. Selected regions of patterns of compounds in the series $Ba_2Eu_{1-x}Pr_xNb_{1-x}Sb_xO_6$ indicating the various symmetries adopted by these compounds. The crosses and continuous lines indicate the observed and calculated intensities which in the case of the two-phase samples includes both the constituent phases and the overall fit. The allowed Bragg reflections are indicated by the vertical markers. The diffraction patterns have been rescaled to better illustrate the changes, with the parent (444) reflection near $2\theta=38.0^\circ$ being $\sim\frac{1}{5}$th as intense as the cubic (400) reflection near $2\theta=21.6^\circ$. The indices given in the figure are those for the listed space group.

Since other members in the $Ba_2LnB'O_6$ series are known to have structures in $I2/m$ and $Fm\bar{3}m$ [7] the possibility that the samples of $Ba_2Eu_{1-x}Pr_xNb_{1-x}Sb_xO_6$ with $0.1\leqslant x\leqslant 0.4$ are a mixture of two phases, $I4/m$ or $R\bar{3}$ with $I2/m$ or $Fm\bar{3}m$, was considered. Extensive testing of all the various possibilities suggested that, for the two oxides with $x=0.1$ and 0.2, the combination of $I4/m$ and $I2/m$ was appropriate. The final *R*-factors for the $I2/m$ and $I4/m$ model for the $x=0.2$ sample, $R_p=4.8\%$ and $R_{wp}=6.2\%$, were noticeably better than those for the next best model of $R\bar{3}$ and $I4/m$, $R_p=7.8\%$ and $R_{wp}=10.3\%$. For the two samples with $x=0.3$ and 0.4 the best fits were obtained with a mixture of $R\bar{3}$ and $I2/m$. For the $x=0.3$ sample $R_p=3.6\%$ and $R_{wp}=4.7\%$ in this model compared to values of 6.4% and 6.0% in the $R\bar{3}/I4/m$ model. The change in phase compositions results in the striking difference between the diffraction patterns of the $x=0.2$ and 0.3 samples illustrated in Fig. 2. For the $x=0.2$ sample the splitting of the cubic (400) reflection near

Table 1
Unit cell parameters and crystallographic details for the end-member compounds of the two series $Ba_2Eu_{1-x}Pr_xNb_{1-x}Sb_xO_6$ and $Ba_2NdNb_{1-x}Sb_xO_6$

Compound	Ba_2EuNbO_6	Ba_2PrSbO_6	Ba_2NdNbO_6	Ba_2NdSbO_6
Space group	$I4/m$	$R\bar{3}$	$I2/m$	$R\bar{3}$
a (Å)	6.00331(4)	6.05270(1)	6.08122(5)	6.04069(1)
b (Å)	$=a$	$=a$	6.04673(5)	$=a$
c (Å)	8.53163(7)	$=a$	8.54026(7)	$=a$
α (°)	90	60.1484(2)	90	60.0998(2)
β (°)	90	$=\alpha$	90.1430(4)	$=\alpha$
γ (°)	90	$=\alpha$	90	$=\alpha$
Ba	4*d* (0, $\frac{1}{2}$, $\frac{1}{4}$)	2*c* (*x*,*x*,*x*)	4*i* (*x*,0,*z*)	2*c* (*x*,*x*,*x*)
x	0	0.2504(1)	0.5014(3)	0.2501(1)
y	$\frac{1}{2}$	$=x$	0	$=x$
z	$\frac{1}{4}$	$=x$	0.2497(2)	$=x$
B (Å^2)	1.03(2)	0.83(1)	0.72(2)	0.61(1)
Ln	2*a* (0,0,0)	1*a* (0,0,0)	2*a* (0,0,0)	1*a* (0,0,0)
B (Å^2)	0.80(2)	0.45(1)	0.44(2)	0.26(1)
B'	2*b* (0,0, $\frac{1}{2}$)	1*b* ($\frac{1}{2}$, $\frac{1}{2}$, $\frac{1}{2}$)	2*d* (0,0, $\frac{1}{2}$)	1*b* ($\frac{1}{2}$, $\frac{1}{2}$, $\frac{1}{2}$)
B (Å^2)	0.80(2)	0.49 (2)	0.30(2)	0.24(1)
O1	4*e* (0,0,*z*)	6*f* (*x*,y,z)	4*i* (*x*,0,*z*)	6*f* (*x*,*y*,*z*)
x	0	0.7210(15)	0.0490(14)	0.7269(13)
y	0	0.2473(18)	0	0.2592(33)
z	0.2665(11)	0.2927(15)	0.2681(10)	0.2776(31)
B (Å^2)	1.55(15)	1.87(11)	0.50(3)	2.33(10)
O2	8*h* (*x*,*y*,0)		8*j* (*x*,*y*,*z*)	
x	0.2941(18)		0.2692(11)	
y	0.2448(22)		0.2718(14)	
z	0		0.9708(9)	
B (Å^2)	2.52(19)		1.22(12)	
R_p (%)	6.4	7.6	6.2	5.6
R_{wp} (%)	7.4	7.2	7.2	7.9

$2\theta = 21.7^\circ$ is more pronounced than that of the (444) reflection near $2\theta = 38.0^\circ$, while in the $x = 0.3$ sample the splitting of the (444) reflection is clearly greater than that of the (400) reflection. The existence of the $I2/m$ monoclinic structure in the two-phase region of $Ba_2Eu_{1-x}Pr_xNb_{1-x}Sb_xO_6$ suggests that the structure changes from $I4/m$ tetragonal to $I2/m$ monoclinic to $R\bar{3}$ rhombohedral with increasing x (see Fig. 3). The sequence of phase transitions seen here is different from that found by Mitchell et al. for $Sr_{1-2x}Na_xLa_xTiO_3$ [16] where the transition from tetragonal ($a^0a^0c^-$) to rhombohedral ($a^-a^-a^-$) structure occurred directly, there being no indication of an intermediate symmetry being adopted.

The two-phase transitions, $I4/m$ to $I2/m$ and $I2/m$ to $R\bar{3}$, must both be discontinuous according to Landau theory [17], and this may account for the co-existence of the two phases. It is also possible that the co-existence of the two phases reflects a solubility limit of the Nb^{5+} and Sb^{5+} cations across the series leading to segregation into two phases with different chemical compositions. To investigate this, variable temperature synchrotron X-ray diffraction patterns of $Ba_2Eu_{0.8}Pr_{0.2}Nb_{0.8}Sb_{0.2}O_6$ were

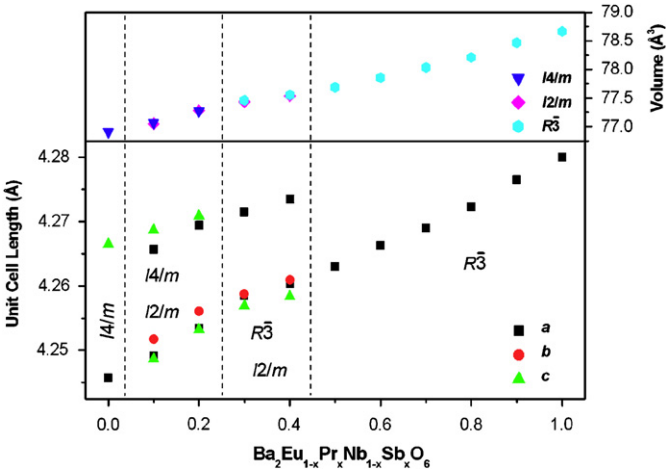

Fig. 3. Variation of the unit cell lengths and volumes for compounds in the series $Ba_2Eu_{1-x}Pr_xNb_{1-x}Sb_xO_6$. The structures that occur for these samples are indicated. The parameters have been reduced to the size of the primitive perovskite structure. Note the systematic variation in volume across the series and the near-identical volumes of the co-existing phases in both two-phase regions.

collected up to a maximum temperature of 500 °C. If the presence of the two phases, evident at room temperature, is caused by an incomplete first-order phase transition it would be expected that the transition to the higher symmetry structure would be completed at some temperature in this range. The diffraction patterns of $Ba_2Eu_{0.8}Pr_{0.2}Nb_{0.8}Sb_{0.2}O_6$ demonstrated the co-existence of two perovskite-type phases up to 500 °C, with the pattern at 500 °C being consistent with two cubic structures. The persistence of the two phases over a temperature range of 500° is a clear indication that the two-phase region in this series is caused by inhomogeneities due to a solubility limit of one or more of the cations in the solution. Despite this phase segregation the volume change across the series $Ba_2Eu_{1-x}Pr_xNb_{1-x}Sb_xO_6$ does not show any significant discontinuities (see Fig. 3). This Vegard-like volume expansion indicates that the segregation in the two-phase region must be relatively small in contrast to the large discontinuities which would be expected if phase segregation was more significant.

In the context of the phase segregation found to occur in this series it is interesting to examine the peak widths of the various single-phase samples in order to better understand any microstrains present. The peak widths of the end-member Ba_2PrSbO_6 compound were very similar to found for an NIST Si-640c sample. This can be seen from a comparison of the (400) and (800) reflections in Ba_2PrSbO_6, that have a full-width at half-maximum intensity (FWHM) of 0.041° and 0.057°, to the Si (133) and (048) reflection, that occur at similar angles and have of FWHM of 0.034° and 0.043°. It was found, however, that the FWHM of the reflections in the samples with $0.1 \leqslant x \leqslant 0.5$ were significantly broader than those in the Ba_2PrSbO_6 ($x = 0$) end member. The FWHM of the (004) and (008) peaks in the $x = 0.5$ sample were 0.064° and 0.144° and for the $x = 0.0$

sample they were 0.041° and 0.057°. It was also found that the samples with composition in the range $0.5 \leqslant x \leqslant 0.9$ exhibited significant anisotropic peak broadening with reflections oriented in the (211) direction being significantly narrower than other peaks in the diffraction pattern. The sample of Ba_2PrSbO_6, by comparison, had significantly less anisotropic peak broadening.

A Williamson–Hall plot [21] analysis was therefore carried out to compare the microstrains present in the $x = 0$ and 0.5 samples by examining the (h00) and (hkl), where $k = l = 2h$, reflections (see Fig. 4). A Williamson–Hall plot relates the measured peak widths of the sample, corrected for instrumental resolution using an appropriate standard, to the mean crystallite size, L, and the distribution of d-spacings, $\Delta d/d$ through the expression $\Gamma\cos(\theta) = (K\lambda/L) + 2(\Delta d/d)\sin(\theta)$ where K is a shape factor close to unity, Γ is the FWHM and λ is the X-ray wavelength. The distribution of d-spacings, i.e. the slope of the plot, is typically interpreted as being related to the degree of microstrain present in a sample where these microstrains can either be a result of structural defects, such as stacking faults, dislocations and intergrowths, or chemical inhomogeneity [22]. The plots for the $x = 0$ and 0.5 samples exhibit significantly different behaviour. For Ba_2PrSbO_6 the plot of both classes of reflections exhibits a very shallow slope indicating that there is only a small amount of microstrain present in this sample; therefore the small amount of peak broadening observed is most likely caused by the crystallite size. By comparison the plot for $Ba_2Eu_{0.5}Pr_{0.5}Nb_{0.5}Sb_{0.5}O_6$ has a much steeper gradient indicating that the large degree of peak broadening present in the diffraction pattern of this sample is caused by the much higher degree of microstrains present. This peak broadening appears to be significantly anisotropic, as indicated by the steeper slope for the (h00) plot compared to the (hkl), where $k = l = 2h$, plot indicates that structural defects strongly contribute to the microstrains although chemical inhomogeneity is likely to also play a significant, but possibly lesser, role in peak broadening in the $0.1 \leqslant x \leqslant 0.5$ samples [22]. It is also worth noting that Ba_2EuNbO_6 also featured a larger degree of peak broadening compared to that found in Ba_2PrSbO_6 suggesting that this compound also has a significant degree of microstrains.

3.2. Structure of $Ba_2NdNb_{1-x}Sb_xO_6$

The second series of mixed Nb–Sb perovskites studied was $Ba_2NdNb_{1-x}Sb_xO_6$. The diffraction pattern of Ba_2NdNbO_6 was well fitted in an $I2/m$ model while the pattern of Ba_2NdSbO_6 showed the structure to be $R\bar{3}$ rhombohedral (see Fig. 5 for selected diffraction patterns and Table 1 for crystallographic details). These results are consistent with previous studies [7]. The patterns for the antimony rich compounds ($x = 0.8$ and 0.9) in the series $Ba_2NdNb_{1-x}Sb_xO_6$ were well fitted by the rhombohedral model. However, the diffraction patterns of the other intermediate compounds ($0.1 \leqslant x \leqslant 0.7$) were not consistent with a single-phase structure, in either monoclinic or rhombohedral symmetry. In all cases the fit using a single-phase model was poor. A significantly better fit was obtained for these compounds using a two-phase model of monoclinic and rhombohedral symmetry (see Fig. 5). It should be noted that the higher resolution available using synchrotron X-ray diffraction was essential in establishing the co-existence of the $R\bar{3}$ and $I2/m$ phases in this series, diffraction patterns obtained using conventional (laboratory) X-ray diffraction were well fitted by single-phase models using either rhombohedral or monoclinic symmetry. The failure to detect the two phases using our

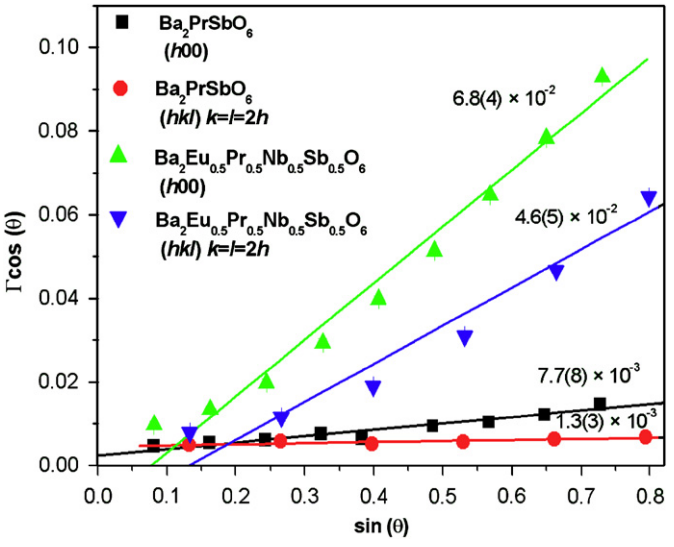

Fig. 4. Williamson–Hall plots for the (h00) and (hkl), where $k = l = 2h$, reflections of Ba_2PrSbO_6 and $Ba_2Eu_{0.2}Pr_{0.8}Nb_{0.2}Sb_{0.8}O_6$ samples. The FWHMs have been corrected for instrumental resolution using an Si-640c standard and the $\Delta d/d$ values are provided for each plot in the figure.

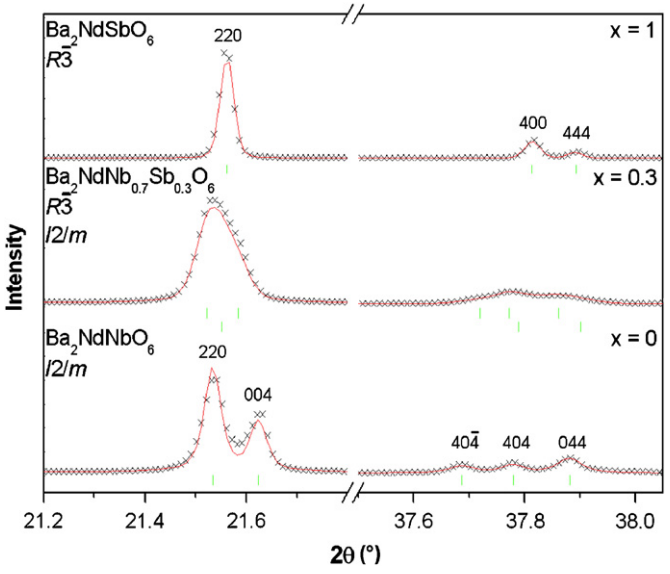

Fig. 5. Selected regions of diffraction patterns of compounds in the series $Ba_2NdNb_{1-x}Sb_xO_6$ illustrating the various symmetries adopted. The format is the same as for Fig. 2.

laboratory based diffractometer is believed to be a consequence of the similarity of the volume of the two end member oxides Ba_2NdNbO_6 and Ba_2NdSbO_6 (78.510(1) and 78.108(6) $Å^3$, respectively, when reduced to the size of the primitive cubic perovskite unit cell). Clearly considerable care is required in order to confirm if single-phase compounds have been formed in such cases.

The existence of this large two-phase region in the $Ba_2NdNb_{1-x}Sb_xO_6$ series (see Fig. 6) is surprising given the relative ease of preparation of the two end member oxides. Phase transitions between structures in $I2/m$ and $R\bar{3}$ have been observed in numerous double perovskites including Ba_2LnSbO_6 [7] and Ba_2LnBiO_6 [23] and are often characterized by a two-phase region. An $I2/m$ to $R\bar{3}$ phase transition is required by Landau theory to be first order [17] and the co-existence of both phases is often characteristic of a first-order transition. That the two-phase region persists over such a wide range of compositions, however, strongly suggests that significant segregation between the two phases occurs. Diffraction patterns obtained for $Ba_2NdNb_{0.5}Sb_{0.5}O_6$ at temperatures of up to 500 °C demonstrated that the sample was two phase over this temperature range, with two cubic phases being found to co-exist at the maximum temperature examined (see Fig. 7). This observation is analogous to that seen in $Ba_2Eu_{0.8}Pr_{0.2}Nb_{0.8}Sb_{0.2}O_6$ and indicates that the two-phase region in both series is a result of insolubility of the cations, albeit at different points in the phase diagram.

Examination of the peak widths of the single-phase samples in the $Ba_2NdNb_{1-x}Sb_xO_6$ series indicates that while Ba_2NdSbO_6 does not contain significant peak broadening, beyond that caused by instrumental resolution, the $x = 0.8$ and 0.9 samples appear to have significant sample induced peak broadening; FWHM of the (400) and (800) peaks of Ba_2NdSbO_6 are 0.033° and 0.043° and 0.087° and 0.192° for $Ba_2NdNb_{0.2}Sb_{0.8}O_6$. Williamson–Hall plots of these samples showed that this additional peak broadening in the Nb^{5+} doped samples appears to be

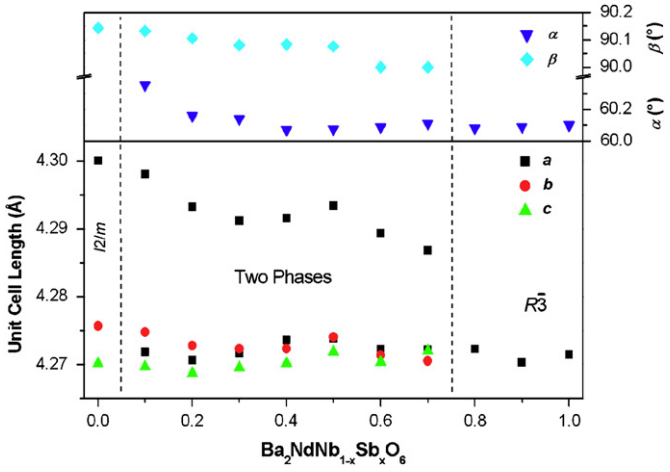

Fig. 6. Lattice parameters for $Ba_2NdNb_{1-x}Sb_xO_6$ indicating the large two-phase region formed in this series. The parameters have been reduced to the size of the primitive perovskite structure.

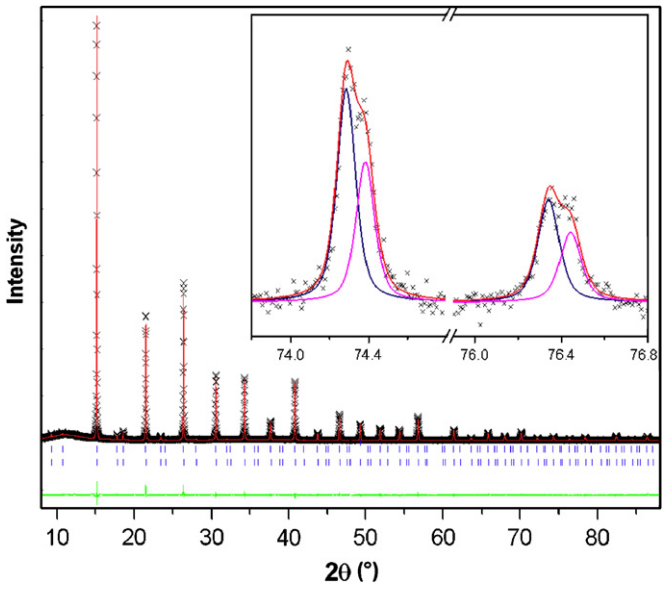

Fig. 7. Synchrotron X-ray diffraction pattern of $Ba_2NdNb_{0.5}Sb_{0.5}O_6$ at 500 °C. The format is the same as for Fig. 1. The insert indicates the calculated intensities of the two cubic phases in the sample and the overall calculated intensity.

a result of increased microstrains in the doped samples similarly to that found in $Ba_2Eu_{1-x}Pr_xNb_{1-x}Sb_xO_6$ samples with $0.1 \leqslant x \leqslant 0.5$. The microstrain, however, of the $Ba_2NdNb_{0.2}Sb_{0.8}O_6$ sample appears to be significantly higher than that found in $Ba_2Eu_{0.5}Pr_{0.5}Nb_{0.5}Sb_{0.5}O_6$. The difference in the microstrains evident in the (h00) and (hkl), $k = l = 2h$, reflections appears to be approximately the same in both samples showing that the additional microstrain in $Ba_2NdNb_{0.2}Sb_{0.8}O_6$ is isotropic. This indicates that the single-phase intermediate samples in the $Ba_2NdNb_{1-x}Sb_xO_6$ series have a higher level of chemical inhomogeneity than those in the $Ba_2Eu_{1-x}Pr_xNb_{1-x}Sb_xO_6$ series. This may be related to the larger two-phase region in the $Ba_2NdNb_{1-x}Sb_xO_6$ series and suggests that the cations present are less compatible in this neodymium series. It should also be noted that while Ba_2NdNbO_6 does appear to have some sample induced peak broadening this is significantly less than that found in Ba_2EuNbO_6, FWHM of 0.047° and 0.074° to 0.065° and 0.145° for the (404) and (808) reflections of Ba_2NdNbO_6 and Ba_2EuNbO_6, respectively. This would seem to suggest that the high degree of sample induced peak broadening in the Ba_2EuNbO_6 sample is caused by factors other than chemical inhomogeneity as these two samples were synthesized using the same method and the chemical behaviour of the cation present in these samples would be expected to be identical under the synthetic conditions used in this work.

3.3. Phase segregation

The synchrotron diffraction patterns of both the $Ba_2NdNb_{1-x}Sb_xO_6$ and $Ba_2Eu_{1-x}Pr_xNb_{1-x}Sb_xO_6$ series demonstrated that a limit in the solubility occurs. Consequently

the chemical composition of selected samples ($x = 0.2$, 0.4, 0.6 and 0.8) was investigated using a combination of SEM and EDX. Backscattered SEM images did not reveal any strongly contrasting regions suggesting the samples were relatively homogeneous on the scale investigated (see Fig. 8). The EDX measurements did not identify any regions that contained only Nb^{5+} or Sb^{5+}, although the estimated standard deviations of the Nb^{5+} content was noticeably, and consistently, higher in the two-phase regions compared to the samples known to be single phase. Higher spatial resolution is required to establish the precise composition of the individual phases present. Nevertheless it is clear from the microscopy and diffraction measurements that a distinct solubility gap occurs in these systems. It is, of course, possible that alternate preparation methods could limit the size of this gap.

That an inhomogeneity in the distribution of Nb^{5+} appears to be related to the two-phase region in both series can be understood in terms of the structures of the different end members. It has previously been argued that the different structures seen in the Ba_2LnNbO_6 and Ba_2LnSbO_6 series are related to differences in the electronic configuration, size and electronegativity [6,7,9] of the Nb^{5+} and Sb^{5+} cations. That different end-member structures are observed suggests that it may not be possible to simultaneously accommodate Nb^{5+} and Sb^{5+} in the same perovskite polymorph. In the series $Ba_2NdNb_{1-x}Sb_xO_6$ it appears that it is only possible to substitute up to 20% Nb^{5+} for Sb^{5+} at the B'-site while maintaining a single-phase rhombohedral structure. At the same time it is not possible to put any significant amount of Sb^{5+} into the monoclinic Ba_2NdNbO_6 structure. Outside these limits significant segregation of the Nb^{5+} and Sb^{5+}, cations into two separate phases occurs. The refinements in the two-phase region indicated that the amount of the two phases present is close to the amount expected if Ba_2NdNbO_6 and Ba_2NdSbO_6 were present in the samples as two separate phases.

The nature of the phase segregation in the $Ba_2Eu_{1-x}Pr_xNb_{1-x}Sb_xO_6$ series is significantly different to that in the neodymium series. In $Ba_2NdNb_{1-x}Sb_xO_6$ the two-phase region appears to be a consequence of the need for Nb^{5+} and Sb^{5+} to adopt different structures. Given the similarities in size and charge of Nb^{5+} and Sb^{5+} (ionic radii of 0.64 and 0.60, respectively [10]) this must reflect a bonding difference. The volumes of the two end-members are very similar indicating the structure has insufficient flexibility to compensate for this. While a solubility limit also exists in the $Ba_2Eu_{1-x}Pr_xNb_{1-x}Sb_xO_6$ oxides tuning of the effective size of the *B*-site lanthanide cation across the series evidently gives additional structural flexibility. This results in a smaller solubility gap but more critically introduces a third monoclinic structure as one part of the two-phase mixture. This suggests that phase transitions from tetragonal to monoclinic and then to rhombohedral occur across this system with partial segregation in the two-phase region. Given that the monoclinic phase is associated with the segregation of the sample into two phases it is not clear whether the monoclinic phase may exist as a single phase between the $x = 0.2$ and 0.3 compositions. While this possibility has not been directly explored it seems unlikely as it would require there to be a region where the Sb^{5+} and Nb^{5+} cations present are completely soluble in the same structure despite the solubility gap clearly present on either side of this region. Regardless of this it would appear that there is a significant region in both series where segregation into two phases is more energetically favourable than forcing the Sb^{5+} and Nb^{5+} cations into an unfavoured geometry.

The solubility of Nb^{5+} in the rhombohedral phase of $Ba_2Eu_{1-x}Pr_xNb_{1-x}Sb_xO_6$ is high, up to 50% of the B'-site cation sites with no segregation into a second phase. There are, however, no single-phase members of this series that contain Sb^{5+} in a tetragonal $I4/m$ structure. The low solubility of Sb^{5+} cations in the niobate structure is believed to be result of Sb^{5+} having a full *d*-shell that does not allow it to participate in π-bonding using these orbitals. π-bonding is considered to be important to stabilizing the tetragonal structure as opposed to rhombohedral symmetry in the $Ba_2LnB'O_6$ series [7]. It is expected that π-bonding would also be important in the monoclinic niobate structure. This observation provides an explanation for the chemical incompatibility of the Nb^{5+} and Sb^{5+} cations. In particular the low solubility of the Sb^{5+} cations in the niobate phases is likely a result of the interruption in the π-bonding in the niobate structure caused by the presence of significant levels of Sb^{5+} cations.

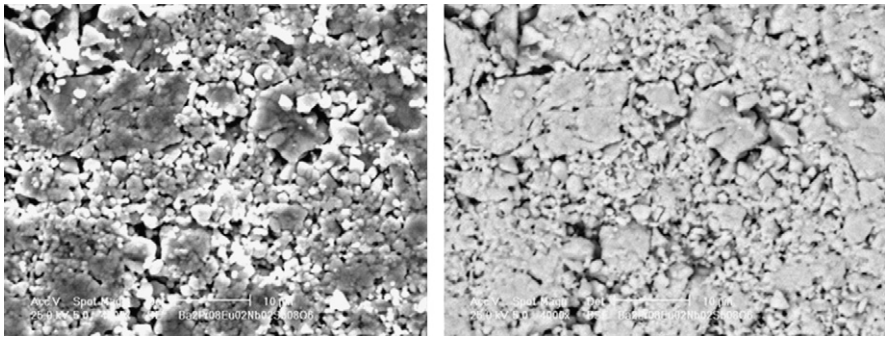

Fig. 8. Secondary (left) and backscattered (right) electron images of $Ba_2Eu_{0.4}Pr_{0.6}Nb_{0.4}Sb_{0.6}O_6$. The lack of contrast in the backscattered image suggests the sample is relatively homogeneous.

4. Conclusion

The phases present in $Ba_2Eu_{1-x}Pr_xNb_{1-x}Sb_xO_6$ and $Ba_2NdNb_{1-x}Sb_xO_6$ have been examined using synchrotron X-ray diffraction. It has been found that the $Ba_2Eu_{1-x}Pr_xNb_{1-x}Sb_xO_6$ series exhibits a series of phases from $I4/m$ tetragonal to $I2/m$ monoclinic to $R\bar{3}$ rhombohedral with increasing x. The monoclinic structure only exists as part of a two-phase mixture with one of the other structures over the range of $0.1 \leqslant x \leqslant 0.4$. Variable temperature X-ray diffraction and energy dispersive X-ray analysis indicates that this segregation is a result of partial segregation of Nb^{5+} and Sb^{5+} into separate phases. The $Ba_2NdNb_{1-x}Sb_xO_6$ series has been found to exhibit extensive phase segregation, consisting of two-phase mixtures of the end-member monoclinic ($x = 0$) and rhombohedral ($x = 1$) structures over the range $0.1 \leqslant x \leqslant 0.7$. This larger solubility gap is presumably due to the lack of tuning of the lanthanide size. In the case of both series the Sb^{5+} cations are found to have much lower solubility in the niobate structure than the Nb^{5+} cations have in the $R\bar{3}$ structure. This is likely to be related to the Sb^{5+} substitution disrupting the π-bonding required to stabilize the tetragonal niobate structure hence making segregation energetically favourable.

Acknowledgments

This work has been partially supported by the Australian Research Council and by AINSE through the provision of an AINSE Postgraduate Award. The work performed at the Australian National Beamline Facility was supported by the Australian Synchrotron Research Program under the Major National Research Facilities program and was performed with the help of Dr. James Hester.

References

[1] R.H. Mitchell, Perovskites Modern and Ancient, Almaz Press Inc., Ontario, 2002.
[2] M. Retuerto, M. García-Hernández, M.J. Martínez-Lope, M.T. Fernández-Díaz, J.P. Attfield, J.A. Alonso, J. Mater. Chem. 17 (2007) 3555–3561.
[3] J.M.D. Coey, M. Viret, S. Molnár, Adv. Phys. 48 (1999) 167–293.
[4] B. Jaffe, R.S. Roth, S. Marzullo, J. Appl. Phys. 25 (1954) 809–810.
[5] R. Guo, L.E. Cross, S.-E. Park, B. Noheda, D.E. Cox, G. Shirane, Phys. Rev. Lett. 84 (2000) 5423–5426.
[6] P.J. Saines, J.R. Spencer, B.J. Kennedy, Y. Kubota, C. Minakata, H. Hano, K. Kato, M. Takata, J. Solid State Chem. 180 (2007) 3001–3007.
[7] P.J. Saines, B.J. Kennedy, M.M. Elcombe, J. Solid State Chem. 180 (2007) 401–409.
[8] W.T. Fu, D.J.W. IJdo, J. Solid State Chem. 178 (2005) 2363–2367.
[9] W.T. Fu, D.J.W. IJdo, J. Solid State Chem. 179 (2006) 1022–1028.
[10] R.D. Shannon, Acta Cryst. A 32 (1976) 751–767.
[11] B.J. Kennedy, C.J. Howard, K.S. Knight, Z. Zhang, Q. Zhou, Acta Cryst. B 62 (2006) 537–546.
[12] J.A. Alonso, E. Mzayek, I. Rasines, J. Solid State Chem. 84 (1990) 16–22.
[13] R. Macquart, B.J. Kennedy, T. Vogt, C.J. Howard, Phys. Rev. B: Condens. Matter 66 (2002), 212102.
[14] A.M. Glazer, Acta Cryst. A 31 (1975) 756–762.
[15] A.M. Glazer, Acta Cryst. B 28 (1972) 3384–3392.
[16] R.H. Mitchell, A.R. Chakhmouradian, P.M. Woodward, Phys. Chem. Miner. 27 (2000) 583–589.
[17] C.J. Howard, B.J. Kennedy, P.M. Woodward, Acta Cryst. B 59 (2003) 463–471.
[18] B.J. Kennedy, C.J. Howard, G.J. Thorogood, M.A.T. Mestreb, J.R. Hester, J. Solid State Chem. 155 (2000) 455–457.
[19] T.M. Sabine, B.J. Kennedy, R.F. Garrett, G.J. Foran, D.J. Cookson, J. Appl. Crystallogr. 28 (1995) 513–517.
[20] B.A. Hunter, C.J. Howard, A Computer Program for Rietveld Analysis of X-ray and Neutron Powder Diffraction Patterns, Lucas Heights Laboratories, 1998.
[21] G.K. Williamson, W.H. Hall, Acta Metall. 1 (1953) 22–31.
[22] J.A. Collado, C. Frontera, J.L. García-Muñoz, C. Ritter, M. Brunelli, M.A.G. Aranda, Chem. Mater. 2003 (2003) 167–174.
[23] W.T.A. Harrison, K.P. Reis, A.J. Jacobson, L.F. Schneemeyer, J.V. Waszczak, Chem. Mater. 7 (1995) 2161–2167.